Biphasic Perchlorate Activation Enabled by a Dinuclear Fe-NHC Complex

Xinyu Xu, Kai Hua, Ming-Tian Zhang*

Center of Basic Molecular Science (CBMS), Department of Chemistry, Tsinghua University, Beijing, 100084 (China)
*Corresponding author. E-mail: mtzhang@mail.tsinghua.edu.cn.

Abstract: Perchlorate, initially perceived as a weakly coordinating counterion rather than a reactive oxidizing reagent due to its kinetic stability, has garnered attention for its potential in microbial systems. In anaerobic conditions, microbes utilize perchlorate as a terminal oxidant for methane oxidation, involving two distinct stages: extraction and release. The biphasic activation process necessitates the collaborative action of multiple enzymes, a phenomenon not extensively explored in artificial systems. To address this, a dinuclear Fe-NHC complex **1** was designed to enable the biphasic activation of perchlorate. Initially, complex **1** extracts the oxidative potential of perchlorate, leading to the formation of Fe(III)-O-Fe(III) complex **2** as the oxidation product. Subsequently, the extracted oxidative potential can be released by photolyzing a mixture of complex **2** and 9,10-dihydroanthracene. Further, an oxidative homocoupling reaction is initiated under anaerobic conditions, achieving the complete biphasic activation of perchlorate using a single artificial catalyst. This work provides new paradigm for constructing biomimetic anaerobic oxidation using kinetically inert high-valent oxygenated acid anions as oxidants.

Introduction

Perchlorate (ClO_4^-), a seemingly simple inorganic anion, has predominantly been regarded as an inert, weakly coordinating counterion, rather than a potent oxidizing reagent, owning to its kinetic inertness in solution.[1] Perchlorate is extensively utilized in coordination chemistry and electrochemistry, especially in the presence of oxidizable transition metal ions.[2] However, perchlorate can serve as a terminal oxidant for methane oxidation in microbes under anaerobic conditions.[3] This process, which unfolds in two distinct stages — the extraction phase and the release phase (Figure 1a) — involves multiple enzymes. During the extraction phase, the oxidative potential of perchlorate is harnessed by the molybdenum-dependent (per)chlorate reductase (PcrAB) in perchlorate reducing bacteria, which sequentially reduces perchlorate to chlorate (ClO_3^-) and chlorite (ClO_2^-).[4] The liberated oxidative potential is then utilized in the anaerobic respiration to oxidize methane to CO_2 via the reverse methanogenesis pathway, mediated by methyl coenzyme M reductase (Mcr) and other enzymes in anaerobic methanotrophic (ANME) archaea , such as *Methanosarcina*.[3] Furthermore, the ClO_2^- formed from perchlorate reduction is further disproportionate to Cl^- and O_2 by the action of chlorite dismutase (Cld);[4] the O_2 evolved from this dismutation process can then be used for aerobic methane activation under anoxic or strictly anaerobic conditions.[3,5] Exploring the replication of biphasic activation process observed in natural systems using a single artificial catalyst presents an intriguing challenge, yet such reactivity remains rare.[6,7] To date, the majority of studies have achieved only the reduction of perchlorate to Cl^- and water.[8] A promising approach to artificial

biphasic perchlorate activation entails employing a bifunctional transition metal catalyst. This catalyst operates by reducing perchlorate to chloride in its reduced state and facilitating the oxidation of alkanes to carbon radical in its high-valent oxo form, as depicted in Figure 1b. This methodology not only allows the utilization of perchlorate as an oxidant but also introduces novel concepts for catalytic anaerobic oxidation and the functionalization of hydrocarbon compounds.

In this work, we developed a dinuclear Fe-NHC (NHC = N-heterocyclic carbene) complex (**1**) to facilitate biphasic activation of perchlorate (Figure 1c). We proposed that the bimetallic center in complex **1** enhances the ClO_4^- coordination and promotes Cl-O bond cleavage step, aided by the electron-rich carbene ligand. The perchlorate reduction reactivity capability of complex **1** was evaluated through stoichiometric reactions with tetrabutylammonium perchlorate ($[^nBu_4N][ClO_4]$), resulting in the formation of a tetranuclear Fe(III)-O-Fe(III) complex **2** as the oxidized product. Broken-symmetry density functional theory (DFT) calculations supported a plausible mechanism for perchlorate activation, confirming the synergistic function of the dual Fe centers in complex **1**. During the release phase, the electronic structure and reactivity of complex **2** were characterized via cycle voltammetry, UV-vis spectroscopy, and time-dependent DFT (TD-DFT) studies. Although complex **2** exhibited ground-state inertness and resistance to reduction, its oxidative potential could be harnessed under photolytic conditions. Ultimately, we developed an oxidative homocoupling reaction utilizing complex **1** as the catalyst and $[^nBu_4N][ClO_4]$ as the sacrificial oxidant, demonstrating the successful biphasic activation of perchlorate by a single artificial catalyst.

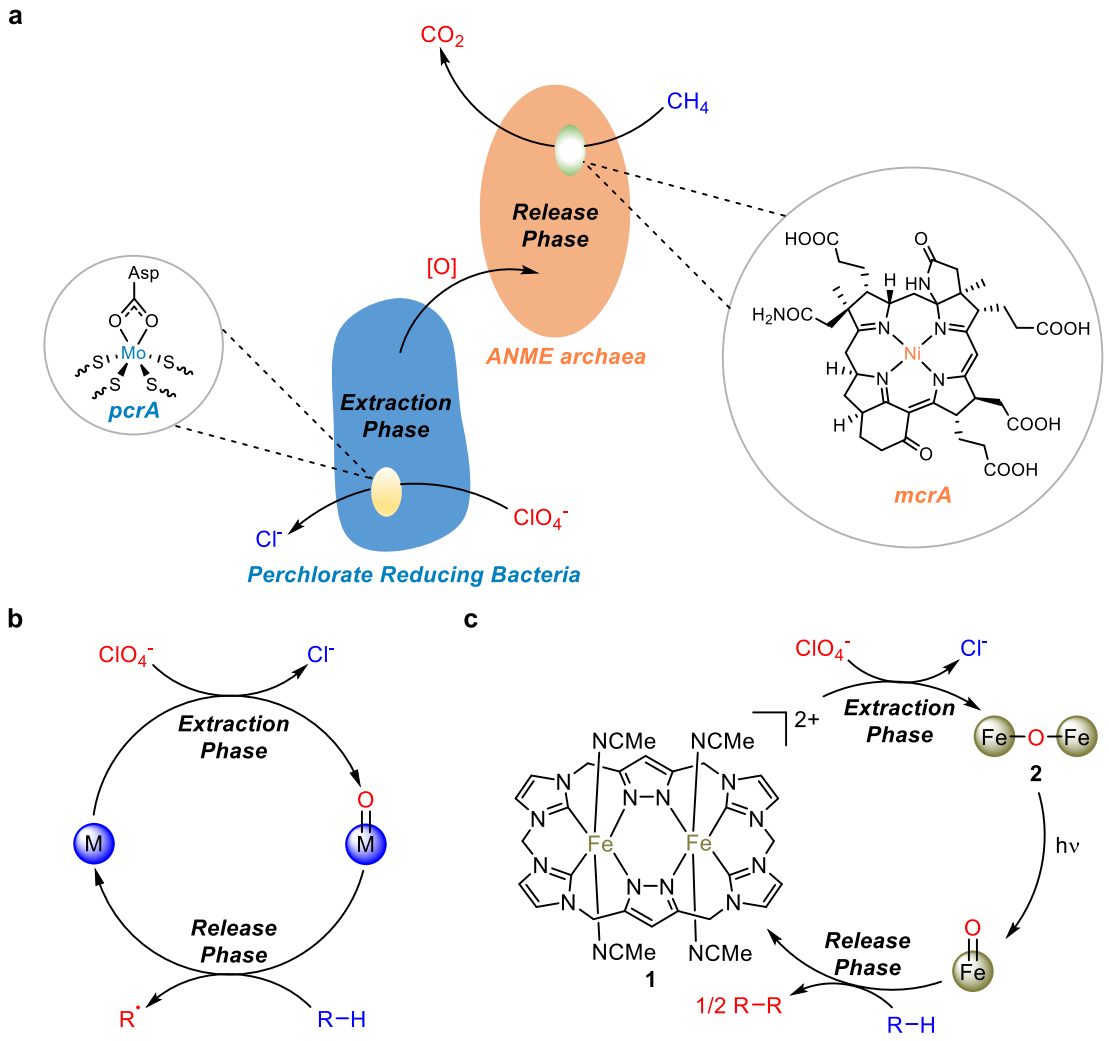

Figure 1. Biphasic perchlorate activation. a, Biphasic perchlorate activation in microbes. During the extraction phase, the oxidative potential stored in perchlorate is extracted by (per)chlorate reductase (PcrAB) in perchlorate reducing bacteria. During the release phase, this extracted oxidative potential is utilized to oxidize methane to CO_2 in anaerobic methanotrophic (ANME) archaea via methyl coenzyme M reductase (Mcr) and other enzymes. **b**, Strategy for artificial biphasic perchlorate activation. **c**, This work: dinuclear Fe-NHC complex enabled biphasic perchlorate activation.

Results and Discussion

Synthesis of Complex 1(PF$_6$)$_2$. The dinuclear iron(II) complex, designated as complex **1**, was synthesized via the reaction of the macrocyclic tetra(imidazolium) salt **H$_6$L(PF$_6$)$_4$** with the common iron precursor Fe(HMDS)$_2$ (HMDS = hexamethyldisilazane) in MeCN (Figure 2a).[9] During the synthesis, moderate solubility of complex **1(PF$_6$)$_2$** in MeCN was noted, leading to its precipitation as the reaction proceeded. This allowed for straightforward isolation of the complex **1(PF$_6$)$_2$** by decantation in 64 % yield. The purity of the obtained compound was conclusively verified by ^{1}H NMR spectroscopy and elemental analysis. Subsequent recrystallization using a mixed MeCN/Et$_2$O solvent facilitated the growth of single crystals suitable for X-ray crystallography, which confirmed the structure of complex

1(PF$_6$)$_2$ as a dinuclear Fe(II)-NHC complex, as shown in Figure 2b. The complex was characterized as low-spin and diamagnetic, with distinct and well-resolved NMR spectra (Figure S2-S7). Electrochemical properties were probed using cycle voltammetry in MeCN, revealing two distinct one-electron redox processes at $E_{1/2}$ = -0.17 V and $E_{1/2}$ = 0.13 V (vs. Fc/Fc$^+$) as illustrated in Figure 2c, comparable with previously reported mononuclear Fe(II)-NHC complexes.[10] These redox events were then attributed to the $Fe^{II}Fe^{II} \rightarrow Fe^{III}Fe^{II}$ and $Fe^{III}Fe^{II} \rightarrow Fe^{III}Fe^{III}$ redox couples, respectively.

Extraction phase. Stoichiometric reaction between complex **1(PF$_6$)$_2$** and [^{n}Bu$_4$N][ClO$_4$] was conducted in CD_3CN solvent with a J. Young NMR tube. Upon heating the reaction mixture at 70 °C, the orange color of complex **1(PF$_6$)$_2$** gradually fade, giving rise to a brown-green solution within 24 h. Monitoring the reaction progress using ^{1}H NMR spectroscopy also unveiled the emergence of a new set of NMR signals within the 2.5-8 ppm range corresponding to the oxidation product as complex **2**. An NMR yield of 91 % was determined for complex **2** at the end of the reaction through the integration the ^{1}H NMR spectra with [^{n}Bu$_4$N]$^+$ as the internal standard (Figure 2d and 2f). Control experiment revealed no reaction in the absence of [^{n}Bu$_4$N][ClO$_4$], underscoring the importance of perchlorate in the formation of complex **2**. In addition, Cl^- was further confirmed as the reduction product through an Ag^+ test in a catalytic reaction (*vide infra*). A dark-brown crystal of complex **2** suitable for single crystal X-ray diffraction analysis can be obtained by layering Et_2O on the top of the reaction mixture and the structure of complex **2** reveals a dimeric structure of complex **1** that bridged by one oxygen atom (Figure 2e). Each complex **2** contains four perchlorate anions, indicating an average oxidation state of +2.5 for each Fe atom or two Fe atoms in +3 oxidation state and the other two Fe atoms in +2 oxidation state. The subsequent description was corroborated by the structural parameter of complex **2**. For Fe atoms that are coordinated in square-pyramidal geometry and bonded to the oxygen atom, the Fe-O distances are 1.7607(4) Å and the Fe-O-Fe angle is 174.75(18)°, which is consistent with the previous value reported by Meyer *et al.* for a tetracarbene coordinated Fe(III)-O-Fe(III) compound.[11] Therefore, the oxidation state of these two Fe atoms were assigned as +3. Sharp ^{1}H NMR signals were clearly observed for complex **2**, indicating strong antiferromagnetic coupling between the two ferric ions. Additionally, the structural parameters of the other two six-coordinated Fe atoms were found to be similar to those measured in complex **1(PF$_6$)$_2$**, supporting the assignment of +2 oxidation state for these two Fe centers. The DFT optimized structure of complex **2** yield a Fe-O distance of 1.77 Å and a Fe-O-Fe angle of 176°, which is consistent with the value obtained by single crystal X-ray diffraction analysis. Spin population analysis showed that spins were localized on two five-coordinated Fe centers and antiferromagnetically coupled with each other, further supporting our oxidation state assignment (Figure S36).

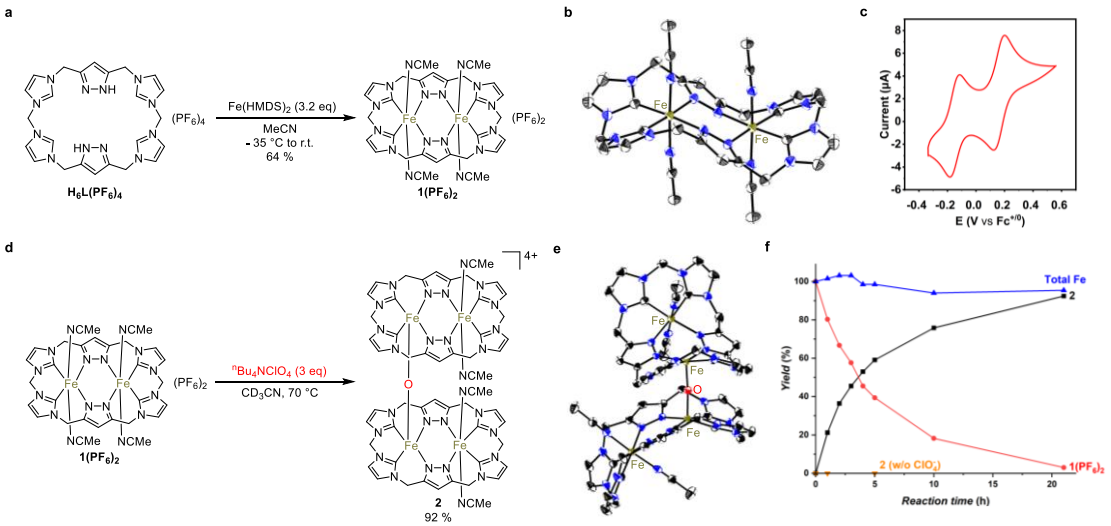

Figure 2. Extraction phase: synthesis, characterization and perchlorate reduction reactivity of complex $\mathbf{1(PF_6)_2}$. a, Synthesis of complex $\mathbf{1(PF_6)_2}$. **b**, Ortep drawing of the cationic fragment of complex $\mathbf{1(PF_6)_2}$. H atoms have been omitted for clarity. Ellipsoids are shown with 50% probability of atoms. **c**, Cyclic voltammograms of the $Fe^{III/II}$ redox couple for complex $\mathbf{1(PF_6)_2}$. **d**, Stoichiometric reaction between complex $\mathbf{1(PF_6)_2}$ and $[^nBu_4N][ClO_4]$. **e**, Kinetic profile of the stoichiometric reaction between complex $\mathbf{1(PF_6)_2}$ and $[^nBu_4N][ClO_4]$. **f**, Ortep drawing of the cationic fragment of complex $\mathbf{2(ClO_4)_4}$. H atoms have been omitted for clarity. Ellipsoids are shown with 50% probability of atoms.

Since other ClO_X^- (x = 1-3) were considered intermediate species in the stoichiometric reduction of perchlorate, reactions between complex $\mathbf{1(PF_6)_2}$ and these anions were also investigated. They were observed to proceed much more rapidly than the reaction between complex $\mathbf{1(PF_6)_2}$ and perchlorate. For instance, a rapid color change to dark-red then dark-brown was observed upon adding 0.33 eq $^nBu_4NClO_3$ to a pre-cooled CD_3CN solution of complex $\mathbf{1(PF_6)_2}$. Monitoring the reaction mixture by ^1H NMR spectroscopy confirmed the formation of complex **2** in 42% yield (Figure S27). Erosion of mass balance was also observed, indicating the presence of over-oxidation. Further addition of $^nBu_4NClO_3$ to excess resulted in the disappearance of complex **2**, accompanied by the precipitation of brown-red solids. Additionally, the formation of NMR silence species was also observed when treating complex $\mathbf{1(PF_6)_2}$ with 4 eq $NaClO_2$. Lastly, reacting complex $\mathbf{1(PF_6)_2}$ with 4 eq $Ca(ClO)_2$ resulted in the smooth formation of complex **2** over a period of 24 h at room temperature. These results indicates that all of these anions (ClO_3^-, ClO_2^-, ClO^-) are more kinetically active than perchlorate and can further oxidize complex **2** even at room temperature (except ClO^-). However, in the stoichiometric reduction of perchlorate, these intermediates must be short-lived and cannot be accumulated in solution due to their high reactivity. Therefore, the clean formation of complex **2** can be achieved by carefully controlling the reaction conditions.[12]

Based on the experimental results discussed above, three possible reaction pathways were proposed for $\mathbf{1(PF_6)_2}$ mediated perchlorate activation (Figure 3). These mechanisms were primary distinguished by the coordination mode between ClO_4^- and complex **1**. In

Pathway 1, ClO_4^- only coordinated to one Fe atom in complex **1**, while in last two pathways, both two Fe atoms was bridged by ClO_4^-. Broken-symmetry DFT calculations were subsequently conducted to estimate the energy barrier of Cl-O cleavage process (**1** → **TS1**-**TS3**) and evaluate the feasibility of these three mechanisms. The computational results indicated that while all three Cl-O cleavage **TSs** should be energetically accessible at reaction temperature, **TS2** and **TS3,** which activate the Cl-O bond in a cooperative manner, were slightly favored over **TS1** by 2-3 kcal/mol. This suggests that both two Fe atoms played important role in perchlorate activation, which was also confirmed by the later discussed fact that the di-Fe catalysts exhibit better catalytic activity than its corresponding mononuclear catalysts with same ligand (*vide infra*).

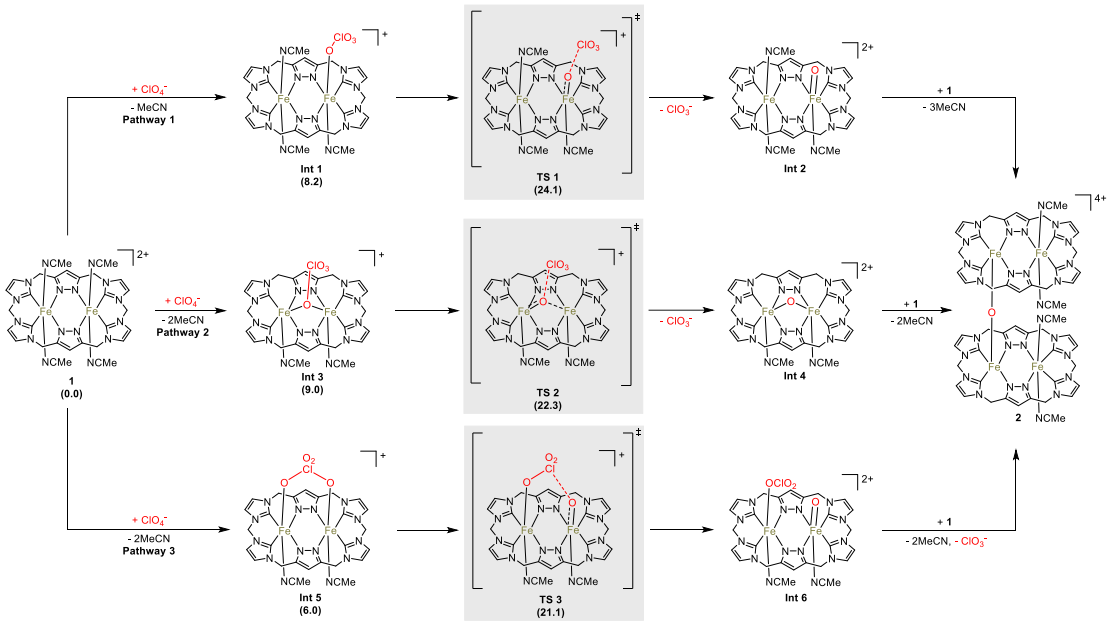

Figure 3. Extraction phase: plausible mechanism of perchlorate activation. DFT calculated Gibbs free energy of selected intermediates and TSs are given in brackets (kcal/mol; calculated at PBE0-D3(BJ)-SMD(MeCN)/SDD-6-311+G(d,p)//B3LYP-D3(BJ)-SMD(MeCN)/SDD-6-31G(d) level of theory).[13-20]

The coordination chemistry between ClO_3^- and complex **1** was also evaluated using DFT method to explain its enhanced reactivity. The coordination of ClO_3^- was always found to be favored over ClO_4^-, regardless of coordination mode considered (Figure S39). Therefore, the experimentally observed improved reactivity of ClO_3^- can be attributed to its stronger nucleophilicity and coordination ability, which facilitate the ligand substitution step.[21] The reactivity of ClO_2^- and ClO^- can also be explained in a similar manner.

Release phase. To release the extracted oxidative potential and achieve catalytic perchlorate reduction, the reactivity of Fe(III)-O-Fe(III) complex **2** was investigated. Surprisingly, complex **2** is highly stable in its ground state and unresponsively toward common single electron reductant, such as Cp_2Fe and Cp^*_2Fe, even in the presence of a proton source. Additionally, complex **2** does also not react with PPh_3, a commonly used oxygen atom transfer reagent. To gain a deeper understanding in the redox reactivity of complex **2**, a cycle voltammetry study was performed in MeCN, demonstrating two

reversible redox couples in the range of -2 V to 1 V (Figure 4a). The redox wave at $E_{1/2}$ = 0 V (*vs.* Fc/Fc$^+$) was assigned to the oxidation of MeCN-coordinated Fe(II) in complex **2** by comparing it with complex **1(PF$_6$)$_2$** and other reported Fe(II)-NHC complexes.[10] The redox wave at $E_{1/2}$ = -1.59 V (vs. Fc/Fc$^+$) was assigned to the reduction of oxygen-coordinated Fe(III) in complex **2** (Figure 5c), which was negatively shift by ~ 200 mV when compared it with the porphyrin derived Fe(III)-O-Fe(III) complex (FeTPP)$_2$O (TPP = 5,10,15,20-tetraphenylporphyrin).[22] This significantly negative value corroborated the reluctance of complex **2** towards reduction and was ascribed to the high oxophilicity of NHC coordinated Fe(III) atom.

To gain deeper insights into the electronic structure of complex **2**, the UV-Vis spectra of complex **2** was recorded and simulated through TD-DFT calculations (Figure 4b). The band at 384 nm (corresponding to calculated λ_{max} = 317 nm) was assigned to an O $\rightarrow$ Fe LMCT transition, supported by the charge density difference plot of excited state 91 (Figure 4b, inset).[23] Other excited states with comparable oscillator strength, such as state 59 and 76 were also analyzed, yielding comparable results (Figure S42 and S43). Building on these computational findings and previous reports[24], we postulated that this LMCT process would weaken the Fe-O bond, leading to the photodisproportionation of complex **2,** generating complex **1** and a Fe(IV)=O intermediate. This Fe(IV)=O intermediate is expected to be kinetically active, releasing its oxidative potential through a hydrogen abstraction (HAT) event with C-H substates, resulting in the formation of a Fe(III)-OH species and a carbon centered radical. Subsequently, complex **2** can be regenerated either through the dimerization of Fe(III)-OH species[25] or the re-oxidation of complex **1** by perchlorate anion (Figure 4c). To validate this hypothesis, complex **2(ClO$_4$)$_4$** was treated with an excess amount of 9,10-dihydroanthracene (**4**) and expose to a purple LED (400 nm, 20 W) for 14 h. Remarkably, the major product observed was the homocoupling product **5**, rather than the commonly observed O-rebounded or aromatized products when using Fe=O as oxidant[6b,25,26], as indicated by the ^{1}H NMR spectrum, suggesting the presence of a hydroanthracene radical intermediate (Figure 4d). Furthermore, achieving a 26 % yield (based on compound **4**) with a turnover number (TON) of 13 indicates that successful regeneration of complex **2** under the experimental conditions. The above experimental results further demonstrate that, with the assistance of light, the dinuclear Fe catalyst can not only acquire oxidative capability from ClO_4^- but also efficiently utilize this energy to oxidize C-H substrates, offering a new perspective on utilizing ClO_4^- as a mild oxidant for C-H activation and functionalization.

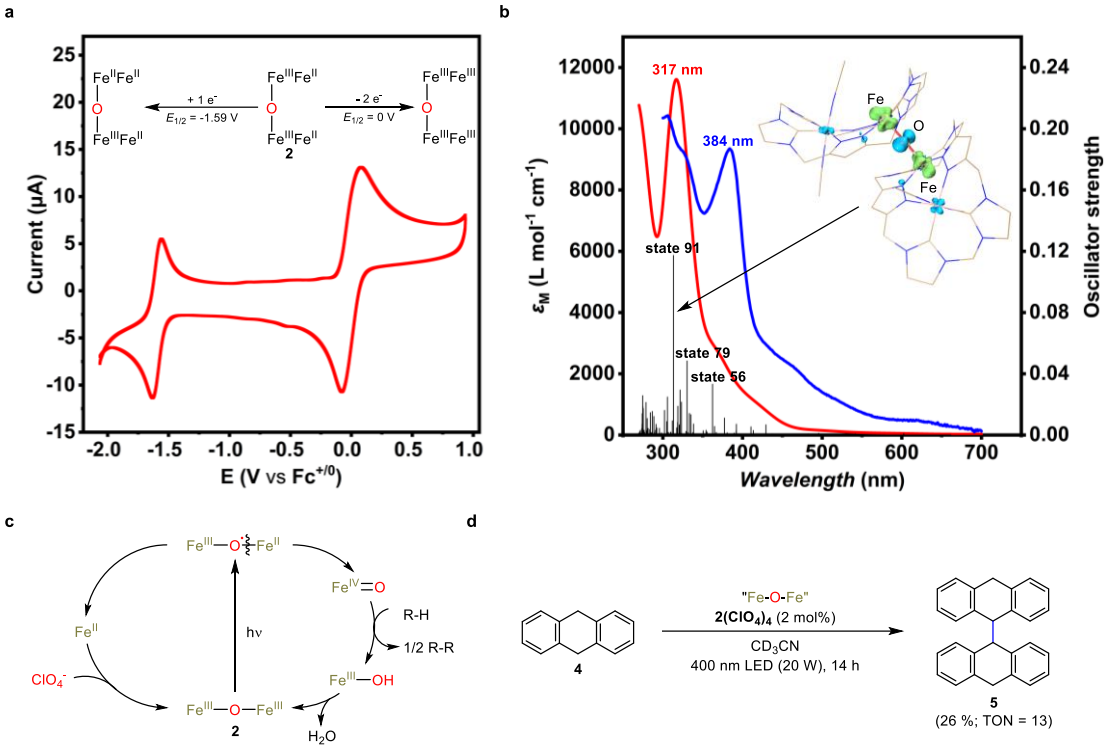

Figure 4. Release phase: reactivity studies of complex 2. a, Cyclic voltammograms of complex **2** recorded in MeCN with 0.1 M [^{n}Bu$_4$N][PF$_6$] (scan rate = 100 mV/s). **b**, Experimental (blue line) and simulated (red line) UV-Vis spectra of complex **2**; black line = calculated oscillator strength of excited states. Inset: Charge density difference plot of excited state 91 (blue = positive; green = negative). **c**, Proposed catalytic cycle. **d**, Release of the oxidative potential of complex **2**.

Oxidative homocoupling reaction under anaerobic conditions. Inspired by the photo-reactivity of complex **2** discovered above, we embarked on the developing a oxidative homocoupling reaction of C-H substrates employing [^{n}Bu$_4$N][ClO$_4$] as the mild oxidant and complex **1(PF$_6$)$_2$** as the molecular catalyst. We were pleased to observe the transformation of C-H substrate **4** into the coupling product **5** in 54 % yield by utilizing 0.25 eq ^{n}Bu$_4$NClO$_4$ and 6 mol% complex **1(PF$_6$)$_2$**, under irradiation by a purple LED (400 nm, 20 W) for 24 h. Extending the reaction time to 72 h increased the yield of product **5** to 78 %, although with catalyst decomposition (Figure 5a). Subsequent testing of these catalyst decomposition products revealed a mere 5% yield for coupling product **5** when used as the catalyst, confirming the homogeneous nature of this homocoupling reaction (Figure S32). Furthermore, control experiments demonstrated the ineffectiveness of simple iron salts, such as Fe(OTf)$_2$, in this homocoupling reaction, emphasizing the pivotal role of the NHC ligand (Table S5, entry 8). While a mononuclear Fe-NHC complex with same ligand scaffold was synthesized and evaluated for this homocoupling reaction, a significant decrease in catalytic efficiency was observed (Figure 5b). Introduction of AgOTf to the post-reaction mixture leading to the formation of white precipitate insoluble in dilute nitric acid, confirming the generation of Cl$^-$ as the reduction product (Figure 5c). Preliminary KIE experiment was conducted to gain mechanistic insights, resulting in a k_H/k_D value equal to 3.7 when treating

the deuterated derivative of compound **4** (**4-d$_4$**) under standard conditions, indicating that HAT process serves as the turn-over limiting step in this reaction (Figure 5d). Additionally, more challenging substrates, such as fluorene (**7**) was also tested and could only be converted into the coupling product **8** by using HFIP (HFIP = hexafluoroisopropanol) as cosolvent (Figure S31). Presumably, HFIP act as Brønsted acid additive, hydrogen bonded or directly protonated the Fe(IV)=O intermediate, thus enhancing its HAT reactivity.[27]

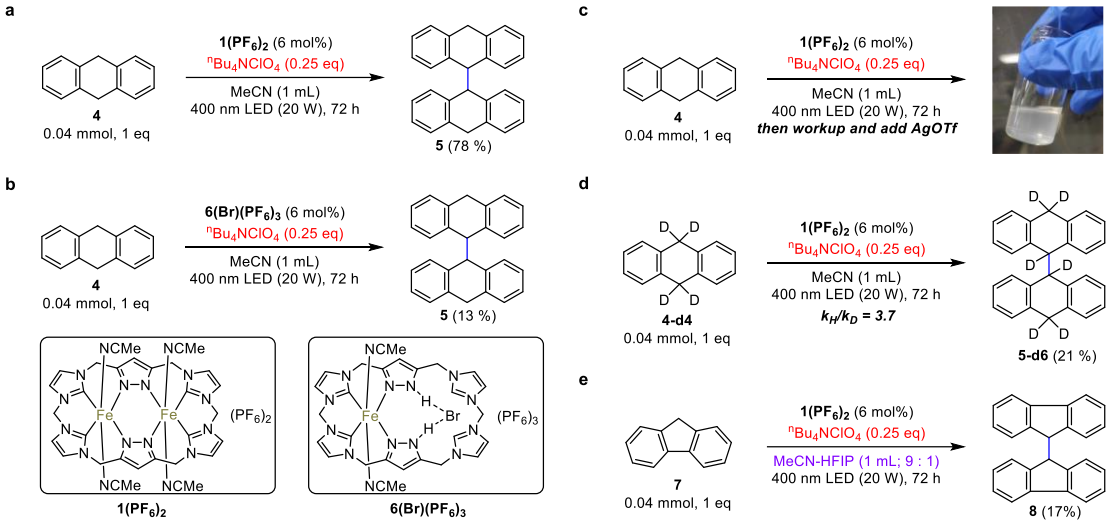

Figure 5. Oxidative homocoupling reactions and mechanistic studies. a, Using **1(PF$_6$)$_2$** as catalyst. **b,** Control experiment by using **6(Br)(PF$_6$)$_3$** as catalyst. **c,** Cl^- detection. **d,** KIE experiment. **e,** Using acidic HFIP as cosolvent.

Conclusion

In this work, biphasic perchlorate activation was achieved by utilizing a dinuclear Fe-NHC complex **1(PF$_6$)$_2$**. Initially, this complex extracted the oxidative capacity of perchlorate, forming the Fe(III)-O-Fe(III) complex **2** and reducing perchlorate to Cl^-. With the assistance of irradiation, the extracted oxidative capacity was released from complex **2**, oxidizing 9,10-dihydroanthracene (**4**) into the homocoupling product **5**. TD-DFT calculation and KIE experiments indicated that complex **2** underwent photoinduced disproportionation to generate a Fe(IV)=O intermediate, which then abstracted a hydrogen atom from the C-H substrates. Furthermore, the HAT reactivity could be enhanced by using acidic HFIP as a cosolvent, providing additional evidence for the presence of a Fe(IV)=O intermediate. While the reactivity of current reaction system remains limited to active C-H substrates, it severed as a conceptual mimic of the anaerobic methane oxidation system and a new perspective on utilizing ClO_4^- as a mild oxidant for C-H activation and functionalization. Future research will focus on developing biphasic perchlorate activation system with a broader substrate scope.

Reference

1. Espenson, J. H. Chapter 1-The problem and Perversity of Perchlorate. In *Perchlorate in the Environment* (Ed.: E. T. Urbansky); Kluwer Academic Publishers / Plenum Press, New York, 2000; pp 1–8.

2. Cotton, F. A. Chapter 13-The Group 17 Elements: F, Cl, Br, I, At. In *Advanced inorganic chemistry*. Wiley, New York, 1999; pp 547–585.
3. (a) Luo, Y.-H.; Chen, R.; Wen, L.-L.; Meng, F.; Zhang, Y.; Lai, C.-Y.; Rittmann, B. E.; Zhao, H.-P.; Zheng, P. Complete perchlorate reduction using methane as the sole electron donor and carbon source. *Environ. Sci. Technol.* **2015**, *49*, 2341−2349. (b) Xie, T.; Yang, Q.; Winkler, M. K.H.; Wang, D.; Zhong, Y.; An, H.; Chen, F.; Yao, F.; Wang, X.; Wu, J.; Li, X. Perchlorate bioreduction linked to methane oxidation in a membrane biofilm reactor: Performance and microbial community structure. *J. Hazard. Mater.* **2018**, *357*, 244–252. (c) Wu, M., Luo, J.-H., Hu, S., Yuan, Z., Guo, J. Perchlorate bio-reduction in a methane-based membrane biofilm reactor in the presence and absence of oxygen. *Water Res.* **2019**, *157*, 572–578. (d) Lv, P.-L.; Shi, L.-D.; Wang, Z.; Rittmann, B.; Zhao, H.-P. Methane oxidation coupled to perchlorate reduction in a membrane biofilm batch reactor. *Sci. Total. Environ.* **2019**, *667*, 9–15. (e) Lv, P.-L.; Jia, C.; Wei, C.-H.; Zhao, H.-P., Chen, R. Efficient perchlorate reduction in microaerobic environment facilitated by partner methane oxidizers. *J. Hazard. Mater.* **2024**, *466*, 133683.
4. Miller, L.G., Baesman, S.M., Carlstroem, C.I., Coates, J.D., Oremland, R.S. Methane oxidation linked to chlorite dismutation. *Front. Microbiol.* **2014**, *5*, 275.
5. (a) Rikken, G. B.; Kroon, A. G. M.; van Ginkel, C. G. Transformation of (per)chlorate into chloride by a newly isolated bacterium: reduction and dismutation. *Appl. Microbiol. Biotechnol.***1996**, *45*, 420−426. (b) Coates, J. D.; Achenbach, L. A. Microbial perchlorate reduction: rocket-fuelled metabolism. *Nat. Rev. Microbiol.* **2004**, *2*, 569−580. (c) Oosterkamp, M. J.; Mehboob, F.; Schraa, G.; Plugge, C. M.; Stams, A. J. Nitrate and (per)chlorate reduction pathways in (per)chlorate-reducing bacteria. *Biochem. Soc. Trans.* **2011**, *39*, 230−235.
6. To the best of our knowledge, only two examples were reported to utilize perchlorate as the oxidant for alkane activation: (a) Suslick, K. S.; Acholla, F. V.; Cook, B. R. Photocatalytic oxidation of hydrocarbons by (5,10,15,20-tetraphenylporphyrinato)manganese(II) perchlorate and periodate. *J. Am. Chem. Soc.***1987**,*109*, 2818–2819. (b) Sarkar, W.; LaDuca, A.; Wilson, R. J.; Szymczak, N. K. Iron-Catalyzed C–H Oxygenation Using Perchlorate Enabled by Secondary Sphere Hydrogen Bonds. *J. Am. Chem. Soc.* **2024**, doi: 10.1021/jacs.3c14433. In both works, the catalytic efficiency was hampered by the inhibition of reduction product Cl^-; expensive silver salts additives were essential to achieve catalytic turnover in these works.
7. Other works that coupled perchlorate reduction to oxygen atom transfer reaction to form stable P-O or S-O bond were also reported in recent years: (a) Ehweiner, M. A.; Wiedemaier, F.; Lajin, B.; Schachner, J. A.; Belaj, F.; Goessler, W.; Mösch-Zanetti, N. C. Nature Inspired Homogeneous Catalytic Perchlorate Reduction Using Molybdenum Complexes. *ACS Catal.* **2021**, *11*, 11754−11761. (b) Bondi, R.; Ehweiner, M. A.; Belaj, F.; Mösch-Zanetti, N. C. Perchlorate reduction catalyzed by dioxidomolybdenum(VI) complexes: Effect of ligand substituents. *J. Catal.* **2022**, *416*, 344−351. (c) Abu-Omar, M. M.; McPherson, L. D.; Arias, J.; Bereau, V. M. Clean and efficient catalytic reduction of perchlorate. *Angew. Chem., Int. Ed.* **2000**, *39*, 4310−4313.
8. (a) Ford, C. L.; Park, Y. J.; Matson, E. M.; Gordon, Z.; Fout, A. R. A Bioinspired Iron Catalyst for Nitrate and Perchlorate Reduction. *Science* **2016**, *354*, 741−743. (b)

Drummond, M. J.; Miller, T. J.; Ford, C. L.; Fout, A. R. Catalytic Perchlorate Reduction Using Iron: Mechanistic Insights and Improved Catalyst Turnover. *ACS Catal.* **2020**, *10*, 3175−3182. (c) Hurley, K. D.; Zhang, Y.; Shapley, J. R. Ligand-Enhanced Reduction of Perchlorate in Water with Heterogeneous Re-Pd/C Catalysts. *J. Am. Chem. Soc.* **2009**, *131*, 14172−14173. (d) Zhang, Y.; Hurley, K. D.; Shapley, J. R. Heterogeneous Catalytic Reduction of Perchlorate in Water with Re-Pd/C Catalysts Derived from an Oxorhenium (V) Molecular Precursor. *Inorg. Chem.* **2011**, *50*, 1534−1543. (e) Ren, C. X.; Liu, J. Y. Bioinspired Catalytic Reduction of Aqueous Perchlorate by One Single-Metal Site with High Stability against Oxidative Deactivation. *ACS Catal.* **2021**, *11*, 6715−6725. (f) Ren, C. X.; Yang, P.; Sun, J. N.; Bi, E. Y.; Gao, J. Y.; Palmer, J.; Zhu, M. Q.; Wu, Y. Y.; Liu, J. Y. A Bioinspired Molybdenum Catalyst for Aqueous Perchlorate Reduction. *J. Am. Chem. Soc.* **2021**, *143*, 7891−7896. (h) Xiong, Z.; Zhao, D.; Pan, G. Rapid and Complete Destruction of Perchlorate in Water and Ion-Exchange Brine Using Stabilized Zero-Valent Iron Nanoparticles. *Water Res.* **2007**, *41*, 3497−3505.

9. ltmann, P. J.; Jandl, C.; Pöthig, A. Introducing a pyrazole/imidazole based hybrid cyclophane: a hydrogen bond sensor and binucleating ligand precursor. *Dalton Trans.* **2015**, *44*, 11278−11281.

10. (a) Anneser, M. R.; Haslinger, S.; Pöthig, A.; Cokoja, M.; Basset, J.-M.; Kühn, F. E. Synthesis and Characterization of an Iron Complex Bearing a Cyclic Tetra-N-heterocyclic Carbene Ligand: An Artificial Heme Analogue? *Inorg. Chem.* **2015**, *54*, 3797−3804. (b) Schremmer, C.; Cordes, C.; Klawitter, I.; Bergner, M.; Schiewer, C. E.; Dechert, S.; Demeshko, S.; John, M.; Meyer, F. Spin-State Variations of Iron(III) Complexes with Tetracarbene Macrocycles. *Chem. Eur. J.* **2019**, *25*, 3918−3929.

11. Meyer, S.; Klawitter, I.; Demeshko, S.; Bill, E.; Meyer, F. A Tetracarbene-Oxoiron(IV) Complex. *Angew. Chem., Int. Ed.* **2013**, *52*, 901−905.

12. Temperature was found to be crucial for the formation of complex **2**. Reactions carried out at higher temperature (> 80 ^{o}C) and extended reaction time resulted in the disappearance of the ligand NMR signal and formation of insoluble brown-red precipitate, presumably due to the uncontrolled, further oxidation of complex **2**.

13. Gaussian 16, Revision A.03, M. J. Frisch, G. W. Trucks, H. B. Schlegel, G. E. Scuseria, M. A. Robb, J. R. Cheeseman, G. Scalmani, V. Barone, G. A. Petersson, H. Nakatsuji, X. Li, M. Caricato, S41 A. V. Marenich, J. Bloino, B. G. Janesko, R. Gomperts, B. Mennucci, H. P. Hratchian, J. V. Ortiz, A. F. Izmaylov, J. L. Sonnenberg, D. Williams-Young, F. Ding, F. Lipparini, F. Egidi, J. Goings, B. Peng, A. Petrone, T. Henderson, D. Ranasinghe, V. G. Zakrzewski, J. Gao, N. Rega, G. Zheng, W. Liang, M. Hada, M. Ehara, K. Toyota, R. Fukuda, J. Hasegawa, M. Ishida, T. Nakajima, Y. Honda, O. Kitao, H. Nakai, T. Vreven, K. Throssell, J. A. Montgomery, Jr., J. E. Peralta, F. Ogliaro, M. J. Bearpark, J. J. Heyd, E. N. Brothers, K. N. Kudin, V. N. Staroverov, T. A. Keith, R. Kobayashi, J. Normand, K. Raghavachari, A. P. Rendell, J. C. Burant, S. S. Iyengar, J. Tomasi, M. Cossi, J. M. Millam, M. Klene, C. Adamo, R. Cammi, J. W. Ochterski, R. L. Martin, K. Morokuma, O. Farkas, J. B. Foresman, and D. J. Fox, Gaussian, Inc., Wallingford CT, 2016.

14. Adamo, C.; Barone, V. Toward Reliable Density Functional Methods without Adjustable Parameters: The PBE0 Model. *J. Chem. Phys.* **1999**, *110*, 6158−6170.

15. (a) Grimme, S.; Antony, J.; Ehrlich, S.; Krieg, H. A consistent and accurate ab initio

parametrization of density functional dispersion correction (DFT-D) for the 94 elements H-Pu. *J. Chem. Phys.* **2010**, *132*, 154104−154119. (b) Grimme, S.; Ehrlich, S.; Goerigk, L. Effect of the damping function in dispersion corrected density functional theory. *J. Comput. Chem.* **2011**, *32*, 1456−1465.
16. Marenich A. V.; Cramer C. J.; Truhlar D. G. Universal solvation model based on solute electron density and on a continuum model of the solvent defined by the bulk dielectric constant and atomic surface tensions. *J. Phys. Chem. B* **2009**, *113*, 6378−6396.
17. (a) Dolg, M.; Wedig, U.; Stoll, H.; Preuss, H. Energy - adjusted ab initio pseudopotentials for the first row transition elements. *J. Chem. Phys.* **1987**, *86*, 866−872. (b) Andrae, D.; Häußermann, U.; Dolg, M.; Stoll, H.; Preuß, H. Energy-adjusted ab initio pseudopotentials for the second and third row transition elements. *Theor. Chem. Acc.* **1990**, *77*, 123−141.
18. Krishnan, R.; Binkley, J. S.; Seeger, R.; Pople, J. A. Self−consistent molecular orbital methods. XX. A basis set for correlated wave functions. *J. Chem. Phys.* **1980**, *72*, 650−654.
19. (a) Becke, A. D. Density-functional thermochemistry. III. The role of exact exchange. *J. Chem. Phys.* **1993**, *98*, 5648−5652. (b) Lee, C.; Yang, W.; Parr, R. G. Development of the Colle-Salvetti correlation-energy formula into a functional of the electron density. Phys. Rev. B: Condens. *Matter Mater. Phys.* **1988**, *37*, 785−789. (c) Stephens, P. J.; Devlin, F. J.; Chabalowski, C. F.; Frisch, M. J. Ab Initio Calculation of Vibrational Absorption and Circular Dichroism Spectra Using Density Functional Force Fields. *J. Phys. Chem.* **1994**, *98*, 11623−11627.
20. (a) Ditchfield, R.; Hehre, W. J.; Pople, J. A. Self - Consistent Molecular - Orbital Methods. IX. An Extended Gaussian - Type Basis for Molecular - Orbital Studies of Organic Molecules. *J. Chem. Phys.* **1971**, *54*, 724−728. (b) Hehre, W. J.; Ditchfield, R.; Pople, J. A. Self-Consistent Molecular Orbital Methods. XII. Further Extensions of Gaussian-Type Basis Sets for Use in Molecular Orbital Studies of Organic Molecules. *J. Chem. Phys.* **1972**, *56*, 2257−2261. (c) Hariharan, P. C.; Pople, J. A. The S42 influence of polarization functions on molecular orbital hydrogenation energies. *Theor. Chim. Acta.* **1973**, *28*, 213−222.
21. Mcpherson, L. D.; Drees, M.; Khan, S. I.; Strassner, T.; Abu-Omar, M. M. Multielectron Atom Transfer Reactions of Perchlorate and Other Substrates Catalyzed by Rhenium Oxazoline and Thiazoline Complexes: Reaction Kinetics, Mechanisms, and Density Functional Theory Calculations. *Inorg. Chem.* **2004**, *43*, 4036−4050.
22. Kadish, K. M.; Larson, G.; Lexa, D.; Momenteau, M. Electrochemical and spectral characterization of the reduction steps of .mu.-oxo-bis(irontetraphenylporphyrin) dimer in dimethylformamide. *J. Am. Chem. Soc.* **1975**, *97*, 282−288.
23. (a) Tian Lu, Feiwu Chen, Multiwfn: A Multifunctional Wavefunction Analyzer, *J. Comput. Chem.* **2012**, *33*, 580−592. (b) Liu, Z. Y.; Lu, T.; Chen, Q. X. An Sp-Hybridized All-Carboatomic Ring, Cyclo[18]Carbon: Electronic Structure, Electronic Spectrum, and Optical Nonlinearity. *Carbon* **2020**, *165*, 461−467.
24. (a) Richman, R. M.; Peterson, M. W. Photodisproportionation of μ-Oxo-bis[(tetraphenylporphinato)iron(III)]. *J. Am. Chem. Soc.* **1982**, *104*, 5795−5796. (b) Wasser, I. M.; Fry, H. C.; Hoertz, P. G.; Meyer, G. J.; Karlin, K. D. Photochemical Organic Oxidations and Dechlorinations with a μ-oxo Bridged Heme/Non-Heme Diiron Complex. *Inorg. Chem.*

2004, *43*, 8272−8281. (c) Rosenthal, J.; Luckett, T. D.; Hodgkiss, J. M.; Nocera, D. G. Photocatalytic Oxidation of Hydrocarbons by a Bis-Iron(III)-μ-Oxo Pacman Porphyrin Using O_2 and Visible Light. *J. Am. Chem. Soc.* **2006**, *128*, 6546−6547. (d) Chen, J.; Stepanovic, S.; Draksharapu, A.; Gruden, M.; Browne, W. R. Non-HemeIron Photocatalyst for Light-Driven Aerobic Oxidation of Methanol. *Angew. Chem., Int. Ed.* **2018**, *57*, 3207−3211.
25. Cordes, C.; Morganti, M.; Klawitter, I.; Schremmer, C.; Dechert, S.; Meyer, F. Disproportionation Equilibrium of a μ-Oxodiiron(III) Complex Giving Rise to C-H Activation Reactivity: Structural Snapshot of a Unique Oxoiron(IV) Adduct. *Angew. Chem., Int. Ed.* **2019**, *58*, 10855−10858.
26. Kupper, C.; Mondal, B.; Serrano-Plana, J.; Klawitter, I.; Neese, F.; Costas, M.; Ye, S.; Meyer, F. Nonclassical Single-State Reactivity of an Oxo-Iron(IV) Complex Confined to Triplet Pathways. *J. Am. Chem. Soc.* **2017**, *139*, 8939−8949.
27. Ehudin, M. A.; Quist, D. A.; Karlin, K. D. Enhanced Rates of C-H Bond Cleavage by a Hydrogen-Bonded Synthetic Heme High-Valent Iron(IV) Oxo Complex. *J. Am. Chem. Soc.* **2019**, *141*,12558−12569.

TOC